Coastal Engineering
Manuscript Draft

Manuscript Number: CENG-D-07-00145

Title: Wind wave measurements and modelling in a fetch-limited semi-enclosed lagoon

Article Type: Research Paper

Section/Category:

Keywords: Wave modelling - Wind waves - Fetch-limited - WaveWatch - Lagoon - New Caledonia

Manuscript Region of Origin:

Abstract: The south-west reef lagoon of New Caledonia is a semi-enclosed basin where, on first approximation, dominating sea state component corresponds to locally generated wind waves. This study aims to evaluate the ability of the wave model WaveWatch III to simulate wind wave distribution in this particular fetch-limited context. Wave parameters were measured in situ by a wave and tide recorder (WTR9 Aanderaa) and by an acoustic Doppler velocimeter (ADV Sontek). Special care was taken in the validation step as, on one hand the wave model did not simulate the propagation of low-frequency oceanic waves inside the lagoon, and on the other hand the measured spectra bear an intrinsic limitation for high frequencies. The approximation of a sea state dominated by wind waves is also verified.

Wind wave measurements and modelling in a fetch-limited semi-enclosed lagoon

Aymeric Jouon [a,*], Jean Pierre Lefebvre [a], Pascal Douillet [a], Sylvain Ouillon [a], Loys Schmied[b]

[a] UR Camelia, IRD, BP A5, 98848 Noumea cedex, New Caledonia
jouon@noumea.ird.nc , douillet@noumea.ird.nc , ouillon@noumea.ird.nc
Phone : (+687) 26 07 27
Fax : (+687) 26 43 26
[b] LSEET-LEPI, Université du Sud Toulon-Var, BP 132, 83957 La Garde cedex, France
loys.schmied@lseet.univ-tln.fr

* corresponding author

Abstract

The south-west reef lagoon of New Caledonia is a semi-enclosed basin where, on first approximation, dominating sea state component corresponds to locally generated wind waves. This study aims to evaluate the ability of the wave model WaveWatch III to simulate wind wave distribution in this particular fetch-limited context. Wave parameters were measured *in situ* by a wave and tide recorder (WTR9 Aanderaa) and by an acoustic Doppler velocimeter (ADV Sontek). Special care was taken in the validation step as, on one hand the wave model did not simulate the propagation of low-frequency oceanic waves inside the lagoon, and on the other hand the measured spectra bear an intrinsic limitation for high frequencies. The approximation of a sea state dominated by wind waves is also verified.

Keywords

Wave modelling - Wind waves - Fetch-limited - WaveWatch - Lagoon - New Caledonia

1. Introduction

In many coastal environments, waves have a major effect on re-suspension of benthic particles (Booth et al., 2000; Prandle et al., 2000). In the South-West Lagoon of New Caledonia (SLNC) re-suspension is the main origin of suspended particles, except during floods which are scarce and generally short (a few days per year at maximum) (Clavier et al., 1995). The SLNC constitutes a reference site for investigating the anthropogenic impacts on a coastal coral reef ecosystem. Since 1996, different parameters have been monitored in order to quantify the hydrodynamic functioning of the lagoon. Amongst others, physical parameters of the water column (Ouillon et al., 2005), turbidity by *in situ* measurements (Jouon et al., submitted) and remote sensing (Ouillon et al., 2004), energy transfer across the barrier reef (Bonneton et al., 2007) have been extensively achieved. Finally, most of these parameters have been used for calibration and validation of numerical model simulations based on the coupling of a 3D hydrodynamic model with a fine particle transport model (Douillet, 1998; Douillet et al., 2001; Jouon et al., 2006). In the previous applications, the 3D hydrodynamic model took into account the tide and the wind but not yet the wave field.

So as to improve the sediment transport numerical model in such a shallow environment, it is necessary to simulate the wave field. The wave model will then be coupled to the hydro-sedimentary model (Grant and Madsen, 1979; Zhang and Li, 1997). Furthermore, a validated wave model is required to simulate the extreme wind seas under cyclonic conditions.

In opened lagoons, ocean waves and wind waves superimpose. In the SLNC, passes are relatively narrow compared to the enclosing reef extension (Fig. 1). Although ocean waves are strongly attenuated by wave breaking and friction over the enclosing reef flat (Bonneton et al., 2007), some of the oceanic waves enter the lagoon through the passes. The local wind intensity coupled to the dimensions of this semi-enclosed basin make it possible for wind to generate waves. A higher limit estimation of sea state characteristics can be assessed following the empirical SMB (Sverdrup, Munk, Bretschneider) method (Bretschneider, 1970). For a 10 m s^{-1} trade wind blowing over a 45 km fetch, during at least 5 hours, the SMB method gives a significant wave height of 1.25 m and a 5 s peak spectral period in infinite depth.

In that context, this study was conducted to evaluate the ability of a wave model to simulate the wind wave field in a coastal semi-enclosed and fetch-limited environment and to quantify oceanic waves entering the domain. The application was conducted by application of the WaveWatch III (WWATCH) model to the SLNC. The model is validated with *in situ* measurements at different locations and under variable wind forcing conditions. In order to obtain measured data that are compatible with model outputs, the deployment of wavemeters required special care. On one hand, the implementation of WWATCH used in this study did not simulate the transformation of oceanic waves, whose frequencies are low (<0.1 Hz). On the other hand, due to attenuation of high frequency components with depth, there is an intrinsic limitation of measured spectra at high frequencies. This last limitation is severe for wind waves in fetch-limited environments. This study illustrates how to select deployment locations for fetch limited wind waves measurements. It also underlines the importance of optimising the choice of the cut-off frequency in order to assess the most important part of the wind wave power spectrum. The comparison of simulated and measured wave spectra is performed over a windowed frequency spectrum.

2. The study site

New Caledonia is a tropical island located in the Western Pacific, about 1500 km east of Australia. It is surrounded by a 22,200 km^2 lagoon. Noumea, the island's main city, is located on the south-west coast. The lagoon area which surrounds Noumea is called the SLNC. The SLNC whose average depth is 17.5 m houses many coral reef islands (Fig. 1). It is separated from the open ocean by a barrier reef incised by deep and narrow passes and distant to the coast from 5 km (northern limit) to 40 km (southern limit) (Fig. 1).

The local wind generates waves in the semi-enclosed lagoon, resulting from the wind action over a fetch of a few tens of kilometres long at maximum. Except for episodes of low wind intensity, the wind wave field is fetch limited. The mean wind waves periods are short (< 5 s). Statistic analysis of meteorological data (Douillet et al., 2001; Ouillon et al., 2005) brought out that the most frequent and long-lasting wind forcing was generated by South-Easterly trade wind regime. A second wind regime was also identified; it corresponds to more variable short lasting Westerly wind events.

3. Material and Methods

3.1. Field measurements

Two devices have been used in this study: a wave and tide recorder (WTR9, Aanderaa) and an acoustic Doppler velocimeter (ADVOcean, Sontek). For each measurement session, they were deployed simultaneously at the same location, mounted on a nonmagnetic structure that assures the sensors to be located 0.5 m over the seabed. Pressure measurements were achieved every 30 minutes.

3.2. Sampling strategy

Since the wave-induced pressure and velocity amplitude decrease exponentially with depth, when the signal to noise ration (SNR) becomes too weak, waves become undetectable at depths greater than a half wave length. According to this limitation, in this study, the maximum deployment depth was estimated under mean trade wind condition to about 5 m from the mean water level.

The short wave period context required taking special care in choosing the location and depth for the *in situ* measurements. The deployment conditions have to meet two opposite criteria; on one hand, the nearer the gauge to the mean water level, the higher the potential cut-off frequency; on the other hand, the probes have to be deployed close to sea-bed to avoid boat collisions during measurement episodes. For these reasons, shallow water areas were selected for deployment.

Due to topographic constrains, the wind intensity and direction vary from the outer lagoon to the head of bays. As the forcing wind in the model was measured in the outer part of the lagoon, we have selected shallow areas in the outer part of the lagoon. These specific locations correspond to the surroundings of coral islands within the lagoon.

Finally the measurement locations had to potentially correspond to areas where the wind waves reach maximum amplitude. This criterion was better met on the windward sides (defined for the main trade wind) of small reefs or small islands, within the main track of the lagoon where the wind waves have the greater fetch.

Three stations were monitored during this study (Fig. 1). WO station was the most southward site and received an oceanic influence through the Boulari pass. WG stations are located approximately at equal distance between the shore and the barrier reef. Two deployments took place nearly at the same location: WG1 from May 19 to June 1, 2006, and WG2 from June 8 to June 11, 2006. For technical reasons, the experiment at WG2 was shorter lived. WT was the closest station to the shore. Summary of the deployment sessions is given in Table 1.

3.3. WTR9 wave parameters estimation

WTR9 samples pressure at the frequency of 2 Hz over 512 s long episodes. The device includes an inboard processing routine that directly estimates the significant height (H_s) and the mean zero crossing period (T_{02}). Prior to deployment, WTR9 required selecting a distance to seabed and a mooring depth amongst fixed intervals for data analysis purpose. WTR9 sets automatically the cut-off frequency (f_c) according to the deployment depth (f_c=0.5 Hz for deployment at 5 m depth).

3.4. ADV wave parameters estimation

The used ADV Sontek is equipped with a high accuracy resonant pressure transducer (Drück). It yields time series sampled at 5 Hz of pressure and tri-dimensional components of velocity over 410 s long episodes.

3.4.1. Non-directional parameters

In a first step, the pressure time-series collected by ADV were used to determine the wave spectrum and non-directional wave parameters. The mean water level (MWL) was estimated from each pressure sample burst as the mean pressure corrected by the sensor elevation from the seabed. The wave-induced pressure time-series were deduced from the pressure time-series corrected from the MWL. From a wave-induced pressure data set, we estimated a one sided-PSD (Power Spectrum Density) of pressure ($P_\eta(f)$) using Welch's averaged modified periodogram method of spectral estimation (Welch, 1967). This PSD is related to the power spectrum $S_{xx}(f)$ by:

$$P_{onesided}(f) = \frac{2}{f_s} S_{xx}(f) \quad \text{for} \quad 0 \le f < \frac{f_s}{2} \tag{1}$$

$$P_{onesided}(f) = 0 \qquad \text{otherwise}$$

where f_s represents the sampling frequency. The final estimated PSD results from the averaging of many PSD estimated on 512 samples segments, which overlap by 25%, and corrected by a Hamming window. The PSD corresponding to the sea surface elevation $P_\eta(f)$ is deduced by application of the transfer function $H_w(f)$ following:

$$P_\eta(f) = \frac{P(f)}{H_w(f)^2} \tag{2}$$

with

$$H_w(f) = \rho g \frac{\cosh(k(h+z))}{\cosh(kh)} \tag{3}$$

and

$$\omega = 2\pi\ f = \sqrt{gk \tanh(kh)} \tag{4}$$

where h is the water depth, z is the distance from the MWL to the sensor, counted positively upward, g is the acceleration of gravity and k is the wave number. For each frequency, the corresponding wave number is computed using the generalized first order dispersion relationship for surface wave (Leblond and Mysak, 1978) and neglecting all ambient currents (eq. 4).

The PSD corresponding to the elevation of the sea surface is hereafter called wave spectrum. It is used to estimate H_s and T_{02} according to:

$$H_s = 4\sqrt{m_0} \tag{5}$$

$$T_{02} = \sqrt{\frac{m_0}{m_2}} \tag{6}$$

where the statistical zero and second moments (m_0, m_2) are estimated from the wave spectrum $P_\eta(f)$ bounded by a low frequency (f_l) and the cut-off frequency (f_c) as follows:

$$m_k = \int_{f_l}^{f_c} P_n(f) f^k df \tag{7}$$

3.4.2. Directional density power spectrum

The directional density power spectrum was assessed using the wave spectrum $P_\eta(f)$, computed from the ADV pressure time-series and the spreading function $D_\eta(f, \theta)$ derived from the tri-dimensional components of velocity measured by the ADV. We assume that the directional density power spectrum results from two decorrelated functions of the elevation of the sea level, $P_\eta(f)$ and $D_\eta(f, \theta)$, according to:

$$P_\eta(f,\theta) = P_\eta(f) . D_\eta(f,\theta) \quad (8)$$

Inboard processing of ADV corrects the pitch and roll, and gives the Northward, Eastward and Upward velocity components according to the local magnetic direction reference. A supplementary correction must be applied by the user in order to convert the velocity components into the geographical referential.

The spreading function $D_\eta(f,\theta)$ was computed from the East- and North- wave orbital velocity data. These measurements were scaled so that they had equal standard deviation and zero mean. The spreading function was estimated by use of routines adapted from the ones developed by the Wave Analysis for Fatigue and Oceanography Group (WAFO Group, 2000). At this stage, the optimal cut-off frequency was selected in order to extend the high frequency bound at the most. The one sided auto and cross power spectral densities of velocity were estimated and the corresponding transfer function $G_w(f)$ was applied:

$$G_w(f) = 2\pi f \frac{\cosh(k(h+z))}{\sinh(kh)} \quad (9)$$

The extended maximum entropy method (EMEM) was used to estimate this function (Hashimoto, 1997). The obtained spreading function $D_\eta(f,\theta)$ was normalized in order to fulfil the condition:

$$\int_0^{2\pi} D_\eta(f,\theta)d\theta = 1 \quad (10)$$

Some artificial low energy peak may appear out of phase with the main peak, when the latter is of high energy. This drawback is inherent to the method, when second order parameters are estimated. The EMEM iteratively seeks the optimal order for the estimation (Hashimoto, 1997). For our dataset, the optimum order was always comprised between 2 and 3. Nevertheless, the eventual appearance of a weak artificial peak cannot conduct to an ambiguity in the main direction.

3.5. Numerical modelling

3.5.1. WaveWatch III

The WWATCH model was implemented to simulate the wave generation and propagation in the SLNC. WWATCH, a 'state-of-the-art' spectral wave model for deep and intermediate water depths, is a third generation wave model developed by Hendrik Tolman at NOAA/NCEP (US National Center for Environmental Prediction). It is based on previous versions of WWATCH (e.g. Tolman, 1989). Version 1.18 of WWATCH (Tolman, 1999) was used in this study. Other similar wave models are also in the public domain, such as the WAM-Cycle 4 explicit model (WAMDIG, 1988; Monbaliu et al., 2000) or the SWAN implicit model (Booij et al., 1999; Ris et al., 1999).

The governing equations for wind wave propagation and generation are well established (see a review of the basic papers and books in Tolman, 1991b). A detailed description of the model is given in Tolman (1989, 1991a, 1991b) and the source terms are fully presented in Tolman and Chalikov (1996). The physics of the model is hereafter briefly presented.

Wind waves are usually described with an energy or variance density F that depends on wave parameters such as the wave number, the intrinsic or relative frequency σ (as observed in a frame of reference moving with the mean current $\vec{U}$), the absolute frequency ω (as observed in a fixed frame) and the wave direction θ. In the linear theory of surface gravity waves on slowly varying depths and currents (e.g. Leblond and Mysak 1978), wave number and frequencies are interrelated in the dispersion relation. After sensitivity analysis on WWATCH-simulated H_s on the SLNC, the choice was made that the implementation of WWATCH in the SLNC does not take into account neither the effects of currents on the wave field, nor the time variations of surface elevation ($\vec{U} = \vec{0}$; $\sigma = \omega$). The dispersion relation is considered as in eq. (4).

In WWATCH, changes of the variance density F due to propagation over varying depths and currents are described using the action balance equation:

$$\frac{\partial N}{\partial t} + \vec{\nabla}.\left[\left(\vec{C}_g + \vec{U}\right)N\right] + \frac{\partial}{\partial \omega}\left(C_\omega N\right) + \frac{\partial}{\partial \theta}\left(C_\theta N\right) = \frac{S_{wind}}{\sigma} + \frac{S_{ds}}{\sigma} + \frac{S_{nl}}{\sigma} + \frac{S_{bf}}{\sigma} \tag{11}$$

where $N = F(x, y; f, \theta; t) / \sigma$ is the action density spectrum, $\vec{C}_g$ is the group velocity, and C_ω and C_θ are the propagation velocities of frequency and direction, respectively, in spectral space. The left-hand terms of eq. (11) represents the local rate of change of wave action density, propagation, and shifting of frequency and direction due to temporal and spatial variations of the mean water depth and the mean current (tides, surges etc.). S_{wind} represents wave growth and decay due to the actions of wind. S_{ds} corresponds to the whitecapping and turbulent dissipation. S_{nl} stands for the nonlinear wave-wave interactions, and S_{bf} represents the bottom friction dissipation. S_{wind} and S_{ds} refers to separate processes, but they may be considered as interrelated, since their balance governs the integral growth characteristics of the wave model. Two source term options are available in WWATCH for these two terms: the first is based on cycles 1 through 3 of the WAM model (WAMDIG, 1988); the second, based on Tolman and Chalikov (1996), is adapted for fetch-limited conditions and was used in this study. Nonlinear wave-wave interactions are modelled using the discrete interaction approximation of Hasselman et al. (1985) for S_{nl}. S_{bf} is modelled by the empirical JONSWAP expression (Hasselman et al., 1973). The model outputs are the directional wave spectrum and several synthetic parameters retrieved through computations based on the directional wave spectrum.

3.5.2. Wave model implementation in the southwest lagoon of New Caledonia

The computation of the numerical model was performed on a laptop computer with an AMD 64 bit 3200+ processor. During the wave recordings, wind was continuously measured at 10 m altitude at one station in the SLNC (see location in Fig. 1). Wind data at Ilot Maître were averaged over 30 min and used as input for the wave model. In the numerical simulation hereafter presented, wind is assumed to be homogeneous over the calculation area.

The implicit assumption of the considered equations is that the medium (depth and current) as well as the wave field vary on time and space scales that are much larger than the corresponding scales of a single wave. The modelled physics do not cover conditions where the waves are severely depth-limited or in the case of wave reflection. The model can be applied outside the surf zone at spatial scales of several hundreds of meters up to several kilometres. The calculations over the SLNC were performed on a Cartesian grid, with a 500 m mesh size in both directions. The grid is the same as those of the hydrodynamics and sediment transport model described in Douillet et al. (2001).

The WWATCH output result used in this study is the given directional wave spectrum. Although WWATCH gives the average period and the significant wave height, as the WTR9 used in this study gives T_{02} and H_s, we chose to compute T_{02} from the directional wave spectrum in order to compare the same statistical parameters from measurements and simulations. For better consistency, and to be capable of performing high frequency filter on the WWATCH data, we chose to do the same for H_s.

3.6. Selecting the shared frequency band

In order to evaluate of the ability of WWATCH to simulate wind waves in the SLNC, we chose to bound the modelled spectra up to the cut-off frequency fixed for measurements and the measured spectra down to the lowest modelled frequency in order to filter the swell. The obtained bandwidth corresponds to the wind wave field truncated by cut-off frequency.

3.6.1. Cut-off frequency

The cut-off frequency (f_c) plays an important role in the representation of the wave spectrum given by the probes used in this study. This parameter has no absolute value, but is only an empirically selected parameter. The cut-off frequency is strongly related to the deployment settings by the surface to depth transfer functions. It is also related to the magnitude of the high frequency components and subsequently to the sensor sensitivity. It is defined as the highest frequency value which corresponds to a component with an acceptable SNR.

As stated before, the value of f_c can only take pre-selected values for the WTR9. For deployment conditions on all sites, it corresponded to a cut-off frequency value of 0.5 Hz.

The choice of a too high cut-off frequency produces a rise in the sea surface elevation PSD at frequencies concomitant to cut-off frequency. The value of the cut-off frequency was chosen to match the highest value that does not produce such side effects. For comparison matter, we also chose to limit the selection to the frequency scale simulated by the model:

$$f_i = 0.11 \times 1.1^{i-1} \qquad (12)$$

where i corresponds to i^{th} frequency class of WWATCH. Following these guidelines, the cut-off frequency was set to 0.46 Hz for the ADV.

3.6.2. Lowest frequency

Oceanic waves propagating inside the SLNC where identified by their low frequencies (<0.1 Hz). No simulated wind waves reach such low frequencies on the SLNC. In order to evaluate the capacity of WWATCH to simulate wind waves on the SLNC, the filtering of frequencies lower than 0.17 Hz was performed on the measured sea surface elevation DSP. This frequency value is low enough not to interfere with wind waves frequencies and high enough to filter swell.

3.7. Swell contribution to SLNC wave field

Filtering non-simulated wave field components (i.e. swell) also allows quantifying the contribution of these components to the global wave field from measurements. It is done by comparing the values of H_s and T_{02} of filtered and non-filtered data. The contribution of filtered wave component to the statistical parameters H_s is computed following the equation:

$$\%H_{s\,swell} = \frac{H_s - H_{sF}}{H_s} \times 100 \tag{13}$$

where subscript F stands for swell filtered data. H_s can be replaced by T_{02} to compute the contribution of the swell to the mean zero crossing period.

3.8. Assessing the ability of WWATCH to simulate wind waves

The agreement between simulations and measurements is assessed through correlation coefficient and linear regression computations over H_s, T_{02} and the mean direction of the wave field (θ_m). The closer the correlation factor is to unity, the better the likelihood between model and measurements. The best least squares fitted line between measurements and simulations yields a regression factor (a) which can be interpreted as an amplification factor between measurements and simulations. The rms error is also computed for quantification of differences between simulations and measurements.

4. Results

4.1. Meteorological conditions during experiments

During the first sequence of measurements (station WO), the wind intensity was globally weak (≤ 5 m s^{-1}) and of variable direction with three episodes of established trade wind from SE of an approximate speed of 10 m s^{-1} (March 31; April 3 and 10) (Fig. 2).

The second sequence of measurements (station WG1: from May 19 to June 1, 2006) was globally characterised by medium intensity trade wind (≤ 10 m s^{-1}) with two major episodes (May 19 and 27) separated by with light western winds (Fig. 2).

Due to its brevity, the third sequence of measurements (station WG2) displayed more homogeneous wind conditions, typical of an established trade winds (≈ 10 m s^{-1}) (Fig. 2).

During the last sequence of measurements (station WT), wind varied slowly following 5 successive stages (Fig. 2). The established Southern wind (≈ 10 m s^{-1}) gradually decreased the next two days, to near zero with a direction shifting to North. The next five days, the direction progressively shifted North-East through South with wind strengthened to velocity comprised between 5 and 10 m s^{-1}. A two days light trade wind episode occurred followed by a one day episode of established trade wind. The deployment session ended with a trade wind episode of variable intensity.

While the wind intensity and the H_s curves show similar trends, no correlation was found between the wind intensity and T_{02} (Fig. 2).

4.2. Post-processing of field measurements

In order to validate the directional spectra obtained by post-processing of ADV measurements, comparisons were firstly conducted between the statistical wave parameters (H_s and T_{02}) yielded by real time in-board computation of the WTR9, and by post-processed computation on pressure data achieved by the ADV without filtering the swell frequency. On all mooring deployments, H_s values were slightly higher on ADV data than on WTR9 (Fig. 2). T_{02} values were always lower on ADV data than on WTR9. This bias is usually weak but can reach higher values for corresponding low H_s phases, as it can be seen with WG1 and WT data. This bias results of the limited versatility for implementing the actual mooring conditions with a WTR9.

In a second step, swell frequencies were withdrawn from ADV measurements. Each applied high pass filter was tuned on the highest frequency of the swell contribution of the specific measured spectra.

Filtering of swell component gave access to the contribution swell to the wave field. The contribution of swell to H_s and T_{02} (Fig. 3) yielded the similar trends. For both parameters, the influence of the swell relatively to the entire wave field was only significant during very low intensity wind episodes or when the wind direction corresponded to a relatively small fetch. When an established trade wind regime was responsible of a well developed wind wave field, the contribution of oceanic waves to overall wave height did not exceed 3% (Fig. 3, station WG2). A threshold value for wind intensity of approximately 5 m s^{-1} (Fig. 3, station WO) before which the contribution of swell to statistic wave field parameters becomes significant (percentage of swell related H_s to the overall H_s around 50%) was identified. The same type of increase in swell contribution to the wave field was identified for specific changes in wind direction (Fig. 3, station WT, red boxed peak). The decrease in wind intensity along with a variation in wind direction, leads to the same feature (Fig. 3, stations WT and WG1, blue boxed peaks).

Filtering the swell component from the wave field allowed us to compare WWATCH simulations and measurements over a shared frequency band. The gain of such filtering for validation purpose is analysed by comparing the results of regression analyses between simulated data against filtered and non filtered measurements.

Comparison between measured and simulated data

4.3.1. H_s and T_{02}

Spectra issued from WWATCH were compared both with non swell filtered and swell filtered measured spectra and windowed over a similar frequency range (Table 2, Fig. 4).

The correlation computed for H_s between WWATCH and ADV was systematically improved after swell filtering, as indicated by higher correlation coefficients (Table 2).

Simulated H_s closely follows the same trend as measured H_s. WWATCH tends to slightly underestimate H_s during light wind episodes (<5 m s^{-1}), while it slightly overestimate H_s during stronger wind episodes (>5 m s^{-1}). This feature is particularly obvious when the results obtained during the deployment with lowest wind velocities (Fig. 4, station WO) and those with the highest wind velocities (Fig. 4, station WG2). Since the study implied to narrow the spectral bandwidth of the simulated data in order to match the filtered field measurements spectra, the simulated H_s were computed from the directional wave spectrum given by WWATCH. Unfortunately, the precision of the used output format is poor; the minimum ASCII value representing 10^{-3} m^2 s at most. This feature is responsible of a truncation that artificially drops to zero the value of H_s during episodes of very weak wind intensity (Fig. 4, stations WO, WG1 and WT).

For all deployments, the correlation coefficients were over 0.90 except for station WG2 where it reached the acceptable value of 0.79. The regression factors for H_s (i.e. the slope of the linear regression relationship between WWATCH results and swell filtered ADV measurements) were slightly over unity. Despite the artificial underestimation of H_s by WWATCH during low intensity wind episodes due to truncation errors, the regression factor values reveals the tendency of WWATCH to globally overestimate H_s. The highest value of regression factor (a=1.19) corresponds to the windiest deployment (WG2), the lowest regression factor (a=1.13) corresponds to the most calm deployment. However, the overestimation of H_s by WWATCH is limited as indicated by the computed value of the rms error that did not exceed 13 cm on all deployments. The mean overestimation of H_s by WWATCH has been computed over all deployments to a value of 33%.

Simulated T_{02} follow the same trend as measured T_{02}. The filtering of swell considerably improved correlations between simulated and measured T_{02}. Every time the WWATCH wave spectrum was artificially null (during light wind episodes, due to truncation errors), the computation of T_{02} could not be performed. However, WO, WG1 and WT show a correlation coefficient superior to 0.7 (Table 2). The regression factors between measured and simulated T_{02} were lower than for H_s. All regression factors for T_{02} are slightly below unity, this indicates that the modelled T_{02} values are slightly lower than the measured ones. However, the rms error did not exceed 0.36 s for all deployments. The mean underestimation of T_{02} by WWATCH has been computed over all deployments to a value of 6%.

4.3.2. Wind waves direction

The directional-spreading of wind waves obtained by ADV and WWATCH are consistent and vary in agreement with the wind intensity (Fig. 5). During higher energy events, the directional spreading of waves measured by ADV is wider than that simulated using WWATCH. This directional spreading is likely caused by a drawback of the computational method. When the EMEM estimates second order parameters, it creates a secondary artificial wave train in the directional spreading function that comes from the opposite direction of the sensed wave train.

The mean direction of wave field did not yield as good correlation coefficient for deployments WO, WG1 and WG2 as the two other statistical wave parameters (Table 3). For these three cases and despite the visual correspondence of wave energy directional spreading (Fig. 5), the rms error reaches high values. On the other hand, for WT deployment, the correlation coefficient is very close to unity (r=0.88). This better correlation obtained at station WT is explained by the wider range of wind direction that occurred during the field measurements (Fig. 2). On the contrary, the poorest correlation coefficient is met for measurements at station WG2, where the range of variation in the wind direction was the weakest (around a mean 100° average direction) (Fig. 5). The limited variation of wind direction combined to the occurrence of a secondary artificial wave train in the directional spreading function due to EMEM likely constitutes the major explanation of these poor results. However, due to increasing computational cost, the resolution of direction is of 30°. Knowing this technical limitation, the values of rms error between modelled and measured wave field direction yield relatively good results.

5. Conclusion

This study has demonstrated the ability of WWATCH to simulate the intensities and direction of the spectral components of a fetch limited wind wave field. The slight overestimation of Hs by WWATCH could be dealt with by adopting a correction factor on the intensity of wind used to force the model as suggested in Tolman (2002). By comparing simulations and filtered spectra of measured data at various locations in the SLNC, it has been shown that the swell contribution has no significant influence on the higher frequency components of the spectra. The general frame of this study constitutes a generic method for improving the validation technique of wave model's ability to simulate wind waves in a fetch-limited context.

In the shallow water domain, special attention must be paid for acquiring data and to process accurate directional spectra. Because of its high versatility, the use of an ADV proved to be necessary for conducting proper field measurements. Since it has no absolute value, the cut-off frequency constitutes one of the most challenging parameters to be determined. Since the cut-off frequency was susceptible to interfere with the representation of the wind wave energy spectrum, it has been tuned *a posteriori*, by analysis of the obtained spectrum. The post processing technique based on the EMEM method has yielded accurate spectra over a large bandwidth.

On one hand, the analysis of the lower frequency bands of the directional wave spectra yielded useful information about the oceanic swell entering the SLNC, and, on the other hand, the analysis of the higher frequency bands has been used to conduct a validation of WWATCH. Finally, it has been proved that neglecting the influence of the swell into the lagoon constituted an acceptable approximation in average wind conditions, for simulating the wave field on the SLNC.

This analysis also suggests that other components of the wave field, such as induced by wave reflection, could be identified through the analysis of the directional spreading of the wave field. Enhancing the spatial resolution of the model could provide a better correspondence in mean wave field direction between simulated and measured data. The use of spatially variable wind forcing in the model could also improve the correspondence of simulated mean wave field direction to the measurements.

The location of measurements had been selected under numerous constrains amongst which the absence of interference of topographic features with the wind wave field. Taking in account the influence of waves on suspended sediment transport near the shore where topographically induced spatial variability of wind are more likely to take place, could require the use of a more sophisticated wind distribution hindcasted by a high-resolution atmospheric model.

Acknowledgments

This study was supported by IRD (UR CAMELIA), by the french scientific Programme National Environnement Côtier (PNEC) and by the french programme ZoNéCo. The authors are grateful to the divers Jean-Louis Menou, Christophe Peignon, Eric Folcher, and Catherine Geoffray and to Captains Sam Tereua, Miguel Clarque and Napoléon Colombani of R.V. CORIS for their contribution during field data acquisition.

References

Booij, N., Ris R.C., Holthuijsen L.H., 1999. A third-generation wave model for coastal regions, Part I, Model description and validation. Journal of Geophysical Research C4 (104), 7649-7666.

Bonneton, P., Lefebvre, J.P., Bretel, P., Ouillon, S., Douillet, P., 2007. Tidal modulation of wave-setup and wave-induced currents on the Aboré coral reef, New Caledonia. Journal of Coastal Research SI50, 762-766.

Booth J.G., Miller R.L., McKee B.A., Leathers R.A., 2000. Wind-induced bottom sediment resuspension in a microtidal coastal environment. Continental Shelf Research 20, 785-806

Bretschneider, C.L., 1970. Wave Forecasting Relations for Wave Generation. Look Lab/Hawaii, 1 (3).

Clavier, J., Chardy P., Chevillon, C., 1995. Sedimentation of particulate matter in the South-West of New Caledonia: spatial and temporal patterns. Estuarine Coastal and Shelf Science 40, 281-294.

Douillet P., 1998. Tidal dynamics of the south-west lagoon of New Caledonia: observations and 2D numerical modelling. Oceanologica Acta 21, 69-79.

Douillet P., Ouillon S., Cordier E., 2001. A numerical model for fine suspended sediment transport in the south-west lagoon of New-Caledonia. Coral Reefs 20, 361-372.

Grant W.D., Madsen O.S., 1979. Combined wave and current interaction with a rough bottom. Journal of Geophysical Research 84 (C4), 1797-1808.

Hasselmann K., Barnett T.P., Bouws E., Carlson H., Cartwright D.E., Enke K., Ewing J.A., Gienapp H., Hasselmann D.E., Kruseman P., Meerburg A., Müller P., Olbers D.J., Richter K., Sell W., Walden H., 1973. Measurements of wind-wave growth and swell decay during the Joint North Sea Wave Project (JONSWAP). Ergänzungsheft zur Deutschen Hydrographischen Zeitschrift A8 (12), 95 pp.

Hasselmann S., Hasselmann K., Allender J.H., Barnett T.P., 1985. Computations and parameterizations of the nonlinear energy transfer in a gravity-wave spectrum, Part I: A new method for efficient computations of the exact nonlinear transfer integral. Journal Physical Oceanography 15, 1369-1377.

Hashimoto N., 1997. Analysis of the directional wave spectrum from field data. In: Philip L.F. Liu (Ed.), Advances in Coastal and Ocean Engineering Vol. 3, World Scientific, Singapore, 103-143.

Jouon, A., Douillet, P., Ouillon, S., Fraunié, P., 2006. Calculations of hydrodynamic time parameters in a semi-opened coastal zone using a 3D hydrodynamic model. Continental Shelf Research 26, 1395-1415.

Jouon, A., Ouillon, S., Douillet, P., Lefebvre, J.P., Fernandez, J.M., Mari, X., (submitted). Spatio-temporal variabilities of concentration and size distribution of Suspended Particulate Matter in a coral reef lagoon. Marine Geology.

Leblond P.H., Mysak L.A., 1978. Waves in the ocean. Elsevier, 602 pp.

Monbaliu J., Padilla-Hernandez R., Hargreaves J.C., Carretero Albiach J.-C., Luo W., Sclavo M., Günther H., 2000. The spectral wave model WAM adapted for applications with high spatial resolution. Coastal Engineering 41, 41-62.

Ouillon, S., Douillet, P., Andréfouët, S., 2004. Coupling satellite data with *in situ* measurements and numerical modeling to study fine suspended sediment transport: a study for the lagoon of New Caledonia. Coral Reefs 23, 109-122.

Ouillon, S., Douillet, P., Fichez, R., Panché, J.Y., 2005. Enhancement of regional variations in salinity and temperature in a coral reef lagoon, New Caledonia. CR Geoscience 337, 1509-1517.

Prandle D., Hargreaves J.C., McManus J.P., R.C. Andrew, Duwe K., Lane A., Mahnke P., Shimwell S., Wolf J., 2000. Tide, wave and suspended sediment modelling on an open coast – Holderness. Coastal Engineering 41 (1-3), 237-267.

Ris R.C., Holthuijsen L.H., Booij N., 1999. A third-generation wave model for coastal regions, Part II: Verification. Journal of Geophysical Research C4 (104), 7667-7681.

Tolman, H.L., 1989. The numerical model WAVEWATCH: a third generation model for the hindcasting of wind waves on tides in shelf seas. Communications on Hydraulic and Geotechnical Engineering, Delft Univ. of Techn., Rep. no. 89-2, 72 pp.

Tolman, H.L., 1991a. Effects of tides and storm surges on North Sea wind waves. Journal of Physical Oceanography 21, 766- 781.

Tolman, H.L., 1991b. A third-generation model for wind waves on slowly varying, unsteady and inhomogeneous depths and currents. Journal of Physical Oceanography 21, 782-797

Tolman, H.L., Chalikov, D.V, 1996. Source terms in a third-generation wind-wave model. Journal of Physical Oceanography 26, 2497-2518.

Tolman, H.L., 1999. User manual and system documentation of WAVEWATCH III version 1.18, NOAA / NWS / NCEP / OMB Technical Note 151, 97 pp. (available at http://polar.wwb.noaa.gov/waves/wavewatch/wavewatch.html)

Tolman, H.L., 2002. Validation of WAVEWATCH III version 1.15 for a global domain. National Oceanic and Atmospheric Administration, National Weather Service, National Centers for Environmental Prediction, OMB Contribution No. 213.

WAFO Group, 2000. A Matlab toolbox for analysis of random waves and loads. Lund University, Lund Institute of Technology, Centre for Mathematic Sciences, Mathematical Statistics, 112 pp.

WAMDIG, 1988. The WAM model - A third generation ocean wave prediction model. Journal of Physical Oceanography 18, 1775-1810.

Welch, P.D., 1967. The use of fast Fourier transform for the estimation of power spectra: a method based on time averaging over short, modified periodograms. Trans. on Audio and Electroacoustics 15, 70–73

Zhang M.Y., Li Y.S., 1997. The dynamic coupling of a third-generation wave model and a 3D hydrodynamic model through boundary layers. Continental Shelf Research 17 (10), 1141-1170.

FIGURE CAPTIONS

Figure 1 SLNC bathymetry and location of wave measurement stations

Figure 2 Wind Forcing, H_s and T_{02} from WTR9 and ADV, for all records

Figure 3 Wind conditions and swell contribution to SLNC wave field for all deployment sessions determined from ADV measurements

Figure 4 Hs and T_{02} from swell filtered ADV and WWATCH, for all records

Figure 5 Direction spreading of WWATCH simulated wind wave field and ADV swell filtered wave field measurements, for all records

Table1

Name of station	Session (yy/mm/dd)	Location (WGS84)	Water Depth (m)
WO	06/03/31-06/04/14	166°29.76' E - 22°25.33' S	3.6
WG1	06/05/19-06/06/01	166°22.79' E - 22°22.17' S	5.5
WG2	06/06/08-06/06/11	166°22.39' E -22°22.03' S	6.2
WT	06/08/08-06/08/21	166°29.77' E - 22°19.04' S	4.7

Table 1 Summary of sessions and locations of wave recording

Table2

		N	swell non filtered a	swell non filtered r	swell filtered a	swell filtered r	swell filtered rms error
Hs (m)	WO	297	0.98	0.89	1.13	0.90	0.13
	WG1	485	1.15	0.91	1.17	0.91	0.08
	WG2	141	1.18	0.79	1.19	0.79	0.12
	WT	592	1.11	0.91	1.14	0.92	0.11
T_{02} (s)	WO	297	0.57	-0.49	0.91	0.71	0.36
	WG1	485	0.86	-0.05	0.95	0.81	0.21
	WG2	141	0.96	0.49	0.96	0.51	0.20
	WT	592	0.84	0.07	0.91	0.76	0.33

Table 2 Parameters of the best fitted linear regression relationship [$y=ax+b$] for H_s and T_{02} between simulations using WWATCH [y] and estimations from swell filtered measurements (right) and from no swell filtered (left) ADV measurements [x].

Table3

		N	a	r	rms error
Θm (°)	WO	240	0.87	0.40	63.209
	WG1	395	0.93	0.40	70.727
	WG2	141	0.90	0.21	30.664
	WT	526	1.11	0.88	24.137

Table 3 Parameters of the best fitted linear regression relationship between mean wave direction θ_m calculated using WWATCH and θ_m estimated from swell filtered ADV measurements

Figure1

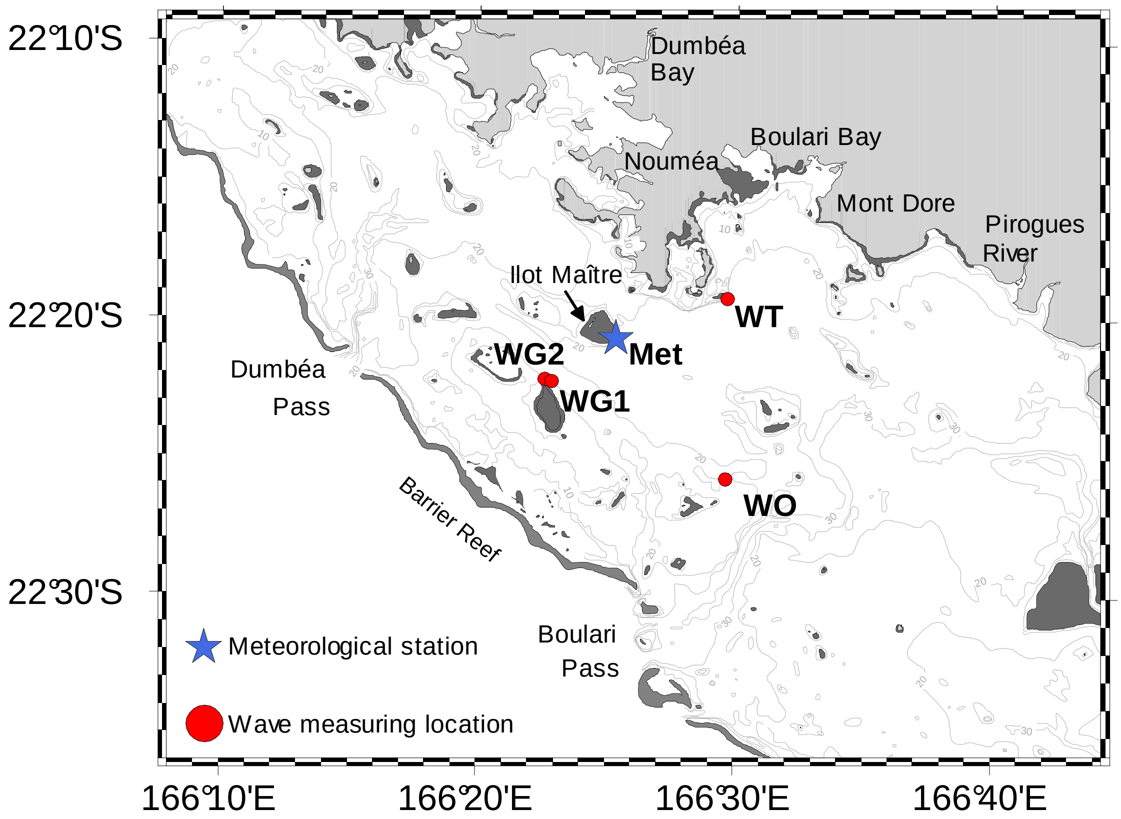
22°10'S
22°20'S
22°30'S
166°10'E
166°20'E
166°30'E
166°40'E
Dumbéa Bay
Boulari Bay
Nouméa
Mont Dore
Pirogues River
Ilot Maître
WT
Met
WG2
WG1
Dumbéa Pass
Barrier Reef
WO
Boulari Pass
Meteorological station
Wave measuring location

Figure2

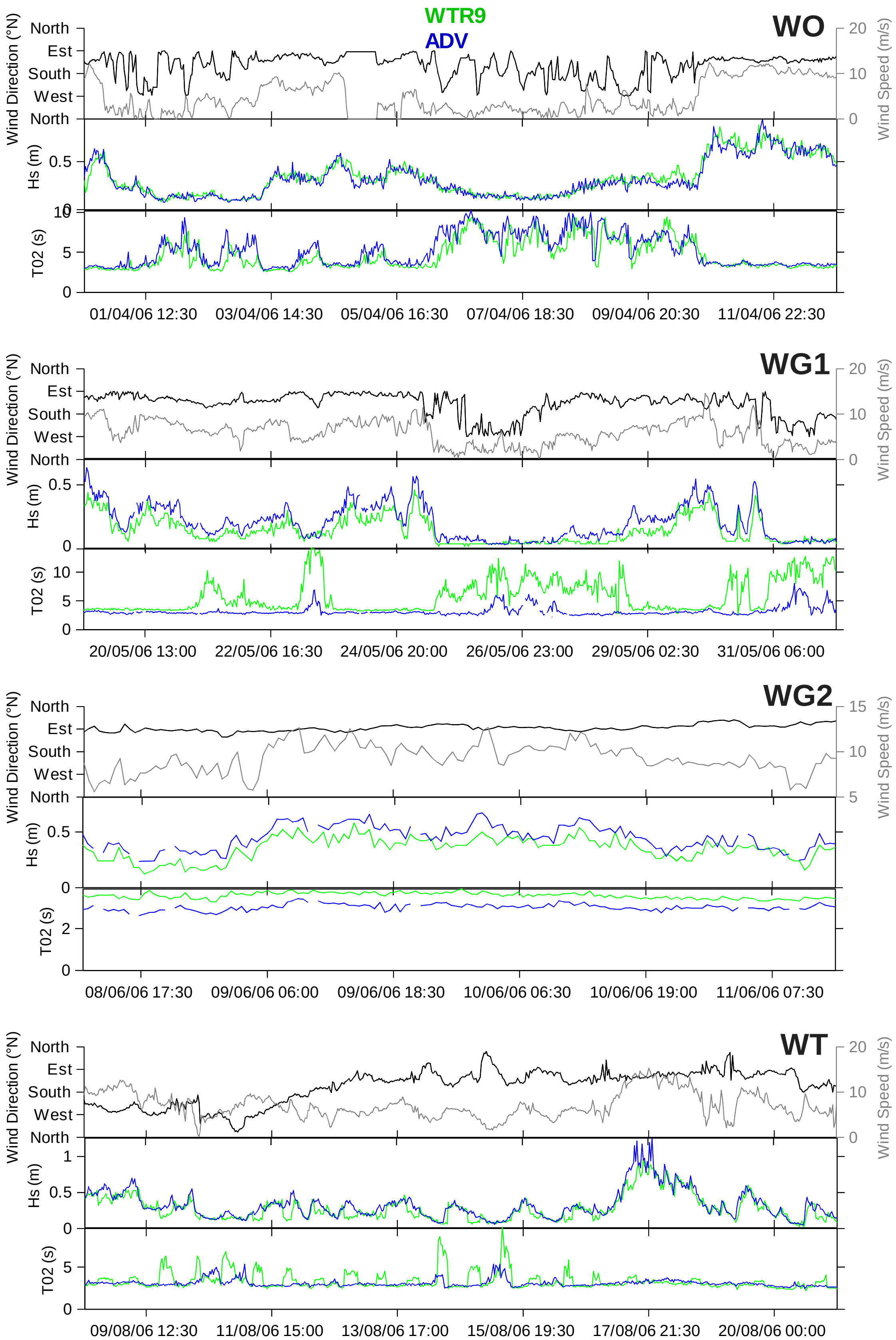

WTR9
ADV
WO
WG1
WG2
WT
Wind Direction (°N)
North
Est
South
West
Wind Speed (m/s)
Hs (m)
T02 (s)
01/04/06 12:30
03/04/06 14:30
05/04/06 16:30
07/04/06 18:30
09/04/06 20:30
11/04/06 22:30
20/05/06 13:00
22/05/06 16:30
24/05/06 20:00
26/05/06 23:00
29/05/06 02:30
31/05/06 06:00
08/06/06 17:30
09/06/06 06:00
09/06/06 18:30
10/06/06 06:30
10/06/06 19:00
11/06/06 07:30
09/08/06 12:30
11/08/06 15:00
13/08/06 17:00
15/08/06 19:30
17/08/06 21:30
20/08/06 00:00

Figure3

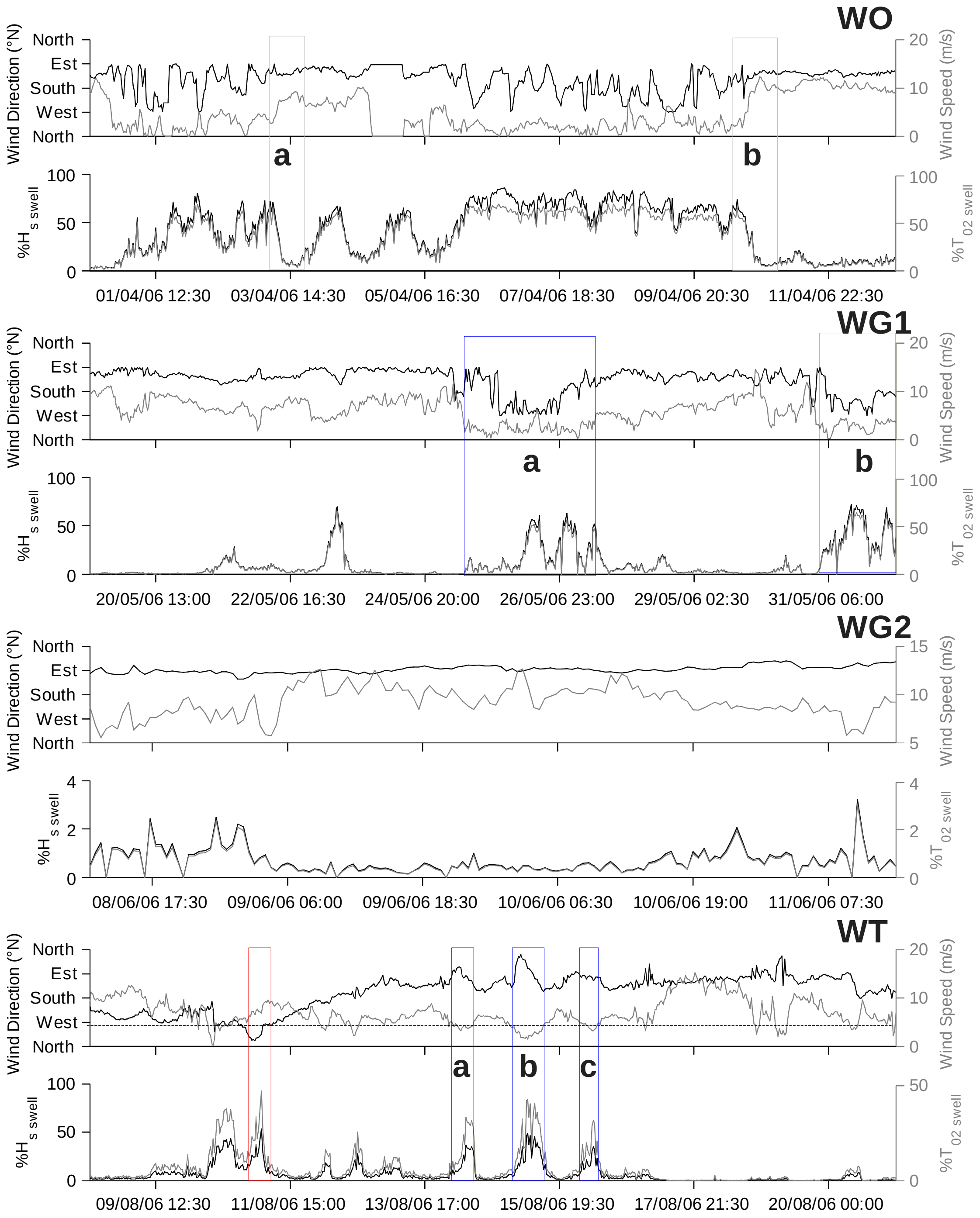

WO
WG1
WG2
WT
Wind Direction (°N)
North
Est
South
West
Wind Speed (m/s)
%H s swell
%T 02 swell
a
b
c
01/04/06 12:30
03/04/06 14:30
05/04/06 16:30
07/04/06 18:30
09/04/06 20:30
11/04/06 22:30
20/05/06 13:00
22/05/06 16:30
24/05/06 20:00
26/05/06 23:00
29/05/06 02:30
31/05/06 06:00
08/06/06 17:30
09/06/06 06:00
09/06/06 18:30
10/06/06 06:30
10/06/06 19:00
11/06/06 07:30
09/08/06 12:30
11/08/06 15:00
13/08/06 17:00
15/08/06 19:30
17/08/06 21:30
20/08/06 00:00

Figure4

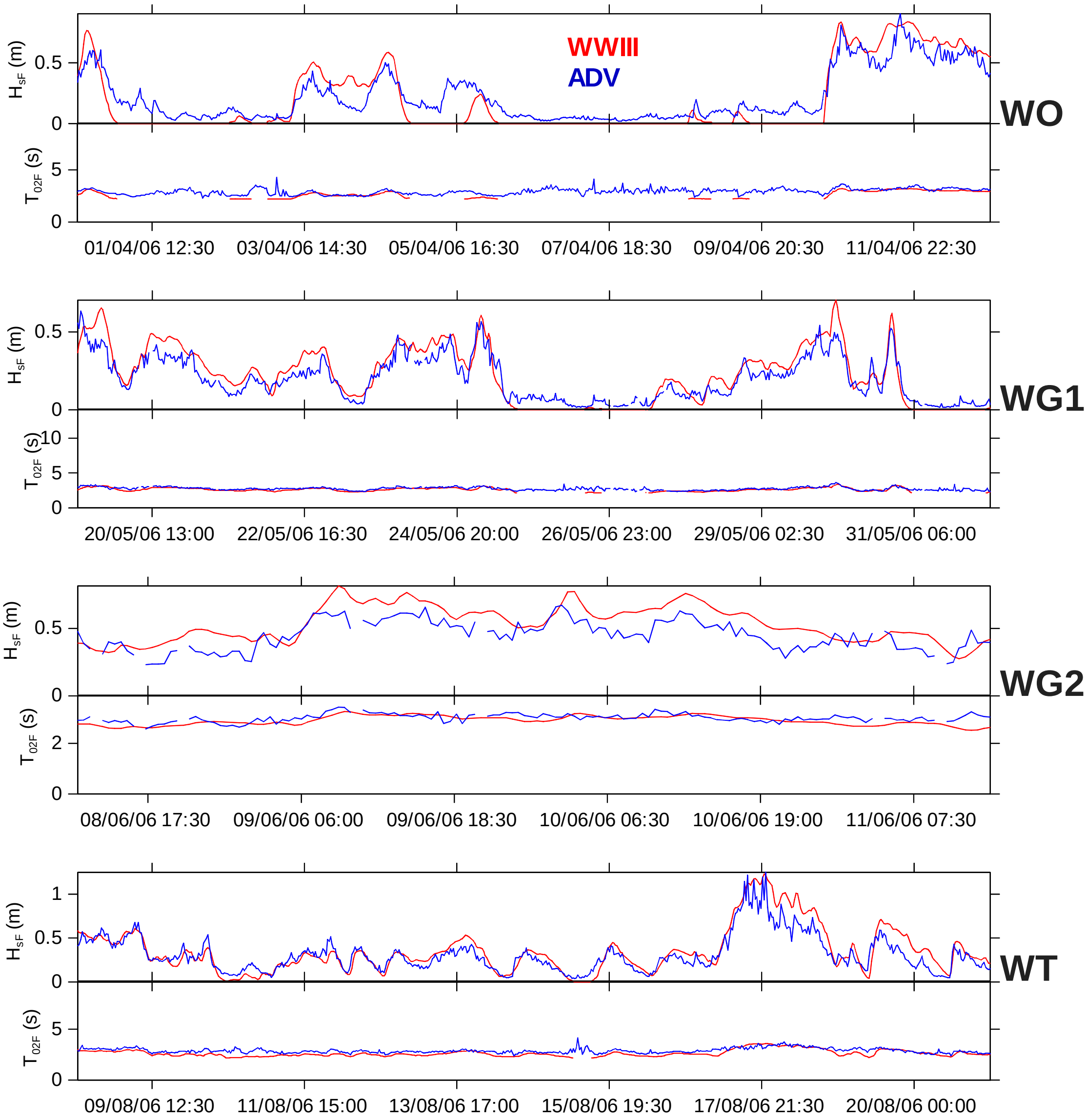

WWIII
ADV
WO
WG1
WG2
WT
H_{sF} (m)
T_{02F} (s)
01/04/06 12:30
03/04/06 14:30
05/04/06 16:30
07/04/06 18:30
09/04/06 20:30
11/04/06 22:30
20/05/06 13:00
22/05/06 16:30
24/05/06 20:00
26/05/06 23:00
29/05/06 02:30
31/05/06 06:00
08/06/06 17:30
09/06/06 06:00
09/06/06 18:30
10/06/06 06:30
10/06/06 19:00
11/06/06 07:30
09/08/06 12:30
11/08/06 15:00
13/08/06 17:00
15/08/06 19:30
17/08/06 21:30
20/08/06 00:00

figure5

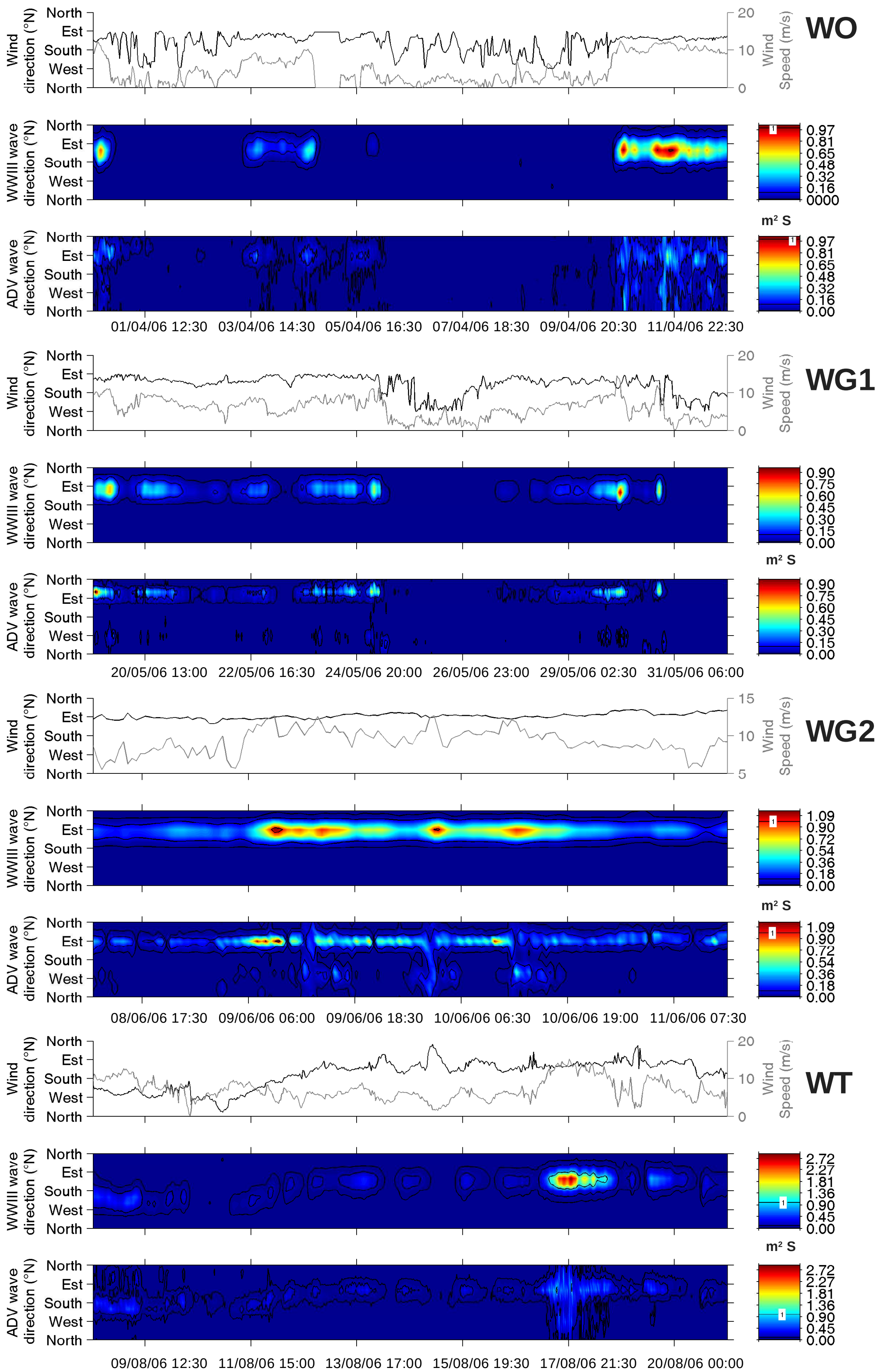

WO
Wind direction (°N)
North
Est
South
West
North
Wind Speed (m/s)
20
10
0
WWIII wave direction (°N)
ADV wave direction (°N)
0.97
0.81
0.65
0.48
0.32
0.16
0000
0.00
m² S
01/04/06 12:30
03/04/06 14:30
05/04/06 16:30
07/04/06 18:30
09/04/06 20:30
11/04/06 22:30
WG1
0.90
0.75
0.60
0.45
0.30
0.15
20/05/06 13:00
22/05/06 16:30
24/05/06 20:00
26/05/06 23:00
29/05/06 02:30
31/05/06 06:00
WG2
15
5
1.09
0.90
0.72
0.54
0.36
0.18
08/06/06 17:30
09/06/06 06:00
09/06/06 18:30
10/06/06 06:30
10/06/06 19:00
11/06/06 07:30
WT
2.72
2.27
1.81
1.36
0.45
09/08/06 12:30
11/08/06 15:00
13/08/06 17:00
15/08/06 19:30
17/08/06 21:30
20/08/06 00:00